RSC Advances

PAPER

View Article Online
View Journal | View Issue

Cite this: *RSC Adv.*, 2021, **11**, 20446

Enhanced bacterial disinfection by CuI–BiOI/rGO hydrogel under visible light irradiation†

Xi Ma,[a] Ziwei Wang,[a] Haoguo Yang,[a] Yiqiu Zhang,[a] Zizhong Zhang,[a] Huaxiang Lin,*[a] Jinlin Long,[a] Xuxu Wang[a] and Qun Lin*[b]

Received 19th April 2021
Accepted 23rd May 2021

DOI: 10.1039/d1ra02966e

rsc.li/rsc-advances

Compared with traditional layered graphene, graphene hydrogels have been used to construct highly efficient visible light-excited photocatalysts due to their particular three-dimensional network structure and efficient electron transport capacity. In this work, CuI–BiOI/rGO hydrogel with excellent photocatalytic antibacterial activity was prepared and its activity against *Escherichia coli* and *Staphylococcus aureus* was evaluated. The result indicates that CuI–BiOI/rGO hydrogel exhibits superior sterilization performance and higher stability than CuI–BiOI and BiOI/rGO, and could completely kill *Escherichia coli* and *Staphylococcus aureus* within 40 min. However, only a small amount of *Escherichia coli* and *Staphylococcus aureus* can be inactivated by CuI–BiOI and BiOI/rGO hydrogels. Graphene hydrogel plays a significant part in enhancing the disinfection activity of CuI–BiOI/rGO hydrogel. Furthermore, the synergistic effect between CuI of p-type semiconductors, as a hole transport layer, and graphene hydrogel greatly increases the separation and transfer efficiency of photogenerated electron holes excited by BiOI, and further improves the disinfection activity of CuI–BiOI/rGO hydrogel.

1. Introduction

It has long been recognized that two-dimensional crystal materials cannot be stable. In 2004, Geim and Novoselov from the University of Manchester in the United Kingdom first obtained single-layer graphene with single atom thickness by a simple micromechanical stripping method.[1] This discovery broke the traditional cognition that graphene cannot exist unsupported. In a single-layer graphene structure, the remaining π electrons in the p_z orbital of each carbon atom can form a large delocalized π bond, where the π electrons can move freely. With the gradual deepening research on graphene, it has been found that graphene exhibits many unique electrical properties, such as electrical conductivity, thermal conductivity and optical characteristics.[2–5] Since graphene is a compound without an energy gap, its π electrons can move freely in layered graphene with a conduction rate of 8×10^5 m s^{-1} that is far superior to that of general semiconductors.[6] The excellent electrical conductivity of graphene enables it to rapidly accept and transmit semiconductor photogenerated electrons.[7,8] However, single-layer graphene causes layer to layer stacking because of π–π conjugation and van der Waals forces between the graphene sheets, which produces a light blocking effect. This effect may reduce the absorption of light and the actual active surface of single-layer graphene. This light blocking effect also inhibits the photocatalytic reaction to a certain extent. Therefore, how to avoid the stacking of layered graphene, thereby increasing the active surface area of graphene and increasing its ability to absorb light are important tasks in the development of graphene photocatalytic applications.[9]

To solve this problem, Shi Gaoquan *et al.* of Tsinghua University prepared a graphene hydrogel by a one-step hydrothermal reduction method in 2010.[10] As shown in Fig. S1,† graphene hydrogel shows three-dimensional network structure in space and appears as a 3D bulk material with good mechanical properties.[11,12] Compared with the layered graphene, graphene hydrogel not only retains the excellent electron transport capability of layered graphene, but also has a unique three-dimensional network structure that allows it to have a developed three-dimensional electron transport path.[13] Due to the developed three-dimensional network structure, the graphene hydrogel can be sufficiently dispersed and supported on the graphene network, which prominently increases the reactive sites.[12,13] For that reason, many researchers are keen to design graphene-based photocatalytic composite materials, and they hope to construct graphene hydrogel composites to replace traditional photocatalysts. Liang Shen and Ziheng Jin *et al.* encapsulated anionic and cationic dyes in wastewater using graphene hydrogel, they found that the hydrogel network provided universal adsorption to those dyes *via* joint electrostatic interaction, chemical interaction and π–π interaction

[a]*College of Chemistry of Fuzhou University, State Key Laboratory of Photocatalysis on Energy and Environment, Fuzhou University, Fuzhou, 350116, China. E-mail: lhx@fzu.edu.cn; Tel: +86 591 22865892*

[b]*Department of Anesthesia, The First Affiliated Hospital, Fujian Medical University, Fuzhou, 350002, China. E-mail: linqun007@163.com*

† Electronic supplementary information (ESI) available. See DOI: 10.1039/d1ra02966e

with the assistance of the immobilized BC01, leading to the enhanced decolorization.[14] Yun Liao, Meng Wang and Dajun Chen prepared a highly porous phosphate-functionalized graphene (HGP) hydrogel electrode material by a two-step process for uranium (U(VI)) electrosorption, the interconnected 3D network structure with graded pores and abundant phosphoric acid groups impart excellent wettability and electrochemical properties to the HGP hydrogel compared to original graphene.[15] These research results show that graphene-based hydrogel materials can use solar energy more effectively.

BiOI, which has a narrow band gap (1.8 eV), can absorb visible light over a wide spectral range.[16] Furthermore, photogenerated holes and electrons in BiOI can be effectively separated by reason of the unique structure of the alternating $[Bi_2O_2]^{2+}$ plate having an I-plate and the internal electric field between the positive and anionic plates.[16–18] Therefore, BiOI has recently attracted broader concerns in the field of water purification under visible light conditions.[19–21] Despite its many advantages, the practical application of BiOI is still limited due to its low efficiency of utilizing visible light.[18,22–24] This is because the hybridization of the valence band Bi 6s and O 2p orbitals makes the carriers easy to recombine.[25,26]

Copper iodide (CuI), as a P-type material with a wide band gap (3.1 eV), has a broad application prospect in the field of photovoltaic devices. In general, in these photovoltaic devices, CuI layer acts as hole transport layer (HTL).[26–30] This is due to its wide band gap of 3.1 eV, providing appropriate level alignment at the interface between the substrate (such as indium tin oxide (ITO)) and the active layer for hole transport.[27] Considering the excellent optical properties of BiOI and the ideal CuI HTL material, effective carrier separation can be achieved in the construction of CuI/BiOI heterostructure.[26] Compared with CuI–BiOI/Cu film,[16] graphene hydrogels can further improve photoelectron generation due to their better electrical conductivity and mechanical properties. Herein, the p-type CuI and graphene hydrogels were selected as hole transport channels and vectors to construct CuI–BiOI/rGO hydrogel, respectively.

In this work, CuI–BiOI/rGO hydrogel was prepared by solvothermal method. Compared with the CuI/BiOI heterostructure and BiOI/rGO hydrogel, the CuI–BiOI/rGO hydrogel shows best photocatalytic sterilization activity under visible light. All of the *Escherichia coli* and *Staphylococcus aureus* were inactivated by the CuI–BiOI/rGO hydrogel under visible light irradiation for 40 min. The results confirm that the synergistic effect of p-type CuI as hole transport channels and rGO hydrogel as electron transport indeed enhances the antibacterial activity.[26]

2. Experimental section

2.1 Materials

The graphene oxide dispersion liqiud was purchased by Nanjing Xianfeng Nanomaterials Technology Co., Ltd, bismuth nitrate pentahydrate ($Bi(NO_3)_3\cdot 5H_2O$, AR), Copper(II) sulfate pentahydrate ($CuSO_4\cdot 5H_2O$, AR), potassium iodide (KI, AR), ethylene glycol (AR) were purchased from Sinopharm Chemical Reagent Co., Ltd, China without any further purification. 5,5-Dimethyl-1-pyrrolidine-*N*-oxide (DMPO, AR) was purchased from McLean Biochemical Technology Co., Ltd The bacteria used in the experiment were cultured in LB broth solution at 37 °C for 18 h, and then diluted to $10^{6.5}$ CFU mL^{-1}. The deionized water is required throughout the antibacterial experiment. After the glass instruments used in the antibacterial experiment is cleaned, it is wrapped and placed in an autoclave, and autoclaved at 121 °C for 20 min.

2.2 Synthesis of CuI–BiOI/rGO hydrogel

Weight 0.1085 g $Bi(NO_3)_3\cdot 5H_2O$ and 0.0559 g $CuSO_4\cdot 5H_2O$ respectively, and add them to 9 mL of ethanol/deionized water mixed solution ($V_{ethanol} : V_{deionized\ water} = 1 : 1$). Then the mixed solution was ultrasonic treated for 30 minutes. Then 15 mL of graphene dispersion (2 mg mL^{-1}) was added to the mixture solution, and 0.1115 g of KI was added to the above mixture. After stirring for 1 h, the mixture solution was transferred into a 50 mL Teflon-lined stainless autoclave and heated at 160 °C for 12 h. Then it was naturally cooled to room temperature, and the synthesized sample was dialyzed with deionized water for 24 h, and repeated two to three times until the concentration of the supernatant obtained by the dialyzing was less than 10 ppm. Finally, CuI–BiOI/rGO hydrogel was obtained by freeze-drying.

2.3 Characterization

The information of the crystal form and crystal plane of the synthetic substance was characterized and analyzed by Bruker D8 X-ray diffractometer (XRD) with Cu Kα radiation operating at 40 mA and 40 kV, The angular scanning range is $2\theta = 5°–80°$. The microscopic morphology and structure state of the material are seen and analyzed by scanning electron microscope (SEM, ZEISS SUPRA 55) and transmission electron microscope (TEM, Tecnai F20), the element mapping of CuI–BiOI/rGO hydrogel is measured by OXFORD EDX 6767. The elemental composition and chemical composition of the sample were tested and analyzed on ESCALAB 250 photoelectron spectrometer (Thermo Fisher Scientific) with 3.0×10^{-10} mbar monochromatic Al Kα radiation ($E = 1486.2$ eV). The laser scanning confocal microscope (LSCM, Leica DMI4000 CS) can apperceive the morphology of the bacteria during the whole reaction. The photochemical test of the material was carried out using a standard three-electrode system at the ZENNIUM electrochemical workstation (Zahner, Germany). The sample was uniformly dispersed and coated on the conductive glass as the working electrode. The test area was about 0.25 cm^2. Pt electrode and Ag/AgCl electrode were used as counter electrode and reference electrode respectively, and 0.2 M Na_2SO_4 was used as electrolyte. Cyclic Voltammetry (CV) and Linear Sweep Voltammetry (LSV) of the composite material were measured in an electrolytic cell containing the above electrodes. The electrolyte is a mixed solution of 0.01 M K_3 $[Fe(CN)_6]$/K_4 $[Fe(CN)_6)$ and 0.5 M KCl. Under the condition of open circuit potential, an AC voltage with an amplitude of 5 mV was applied in the frequency range of 0.5 kHz, 1 kHz and 1.5 kHz for testing. The optical properties of the material are tested and analyzed by Fluorescence Spectrophotometer (PL, F-7000).

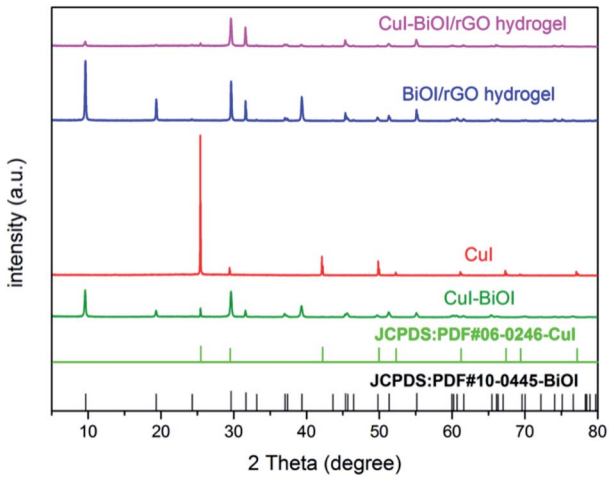

Fig. 1 XRD patterns of CuI, CuI–BiOI, BiOI/rGO hydrogel, CuI–BiOI/rGO hydrogel.

2.4 Photocatalytic disinfection performance

The photocatalytic antibacterial activity of CuI–BiOI/rGO hydrogel, BiOI/rGO hydrogel and CuI–BiOI was mainly evaluated with *Escherichia coli* K-12 as a model bacteria. Before the experiment, the bacteria were cultured in 37 °C nutrient medium. First, 40 mL PBS mixed bacterial fluid ($1 \times 10^{6.5}$ CFU mL^{-1}) was stirred evenly in the photocatalytic reactor, and then add 20 mg of catalyst for illumination. The light source uses the visible light of a 300 W xenon lamp ($\lambda \geq 420$ nm). 0.5 mL of light-treated *Escherichia coli* solution was absorbed every 10 minutes, diluted to a certain multiple, then spread on the newly prepared AGAR plate and cultured at 37 °C for 24 h at a constant temperature.

2.5 Laser scanning confocal microscopy (LSCM) observation of bacteria

Laser scanning confocal microscope is often used to observe and analyze the three-dimensional structure of cells without damage. In this work, the bacteria were placed in a glass Petri dish after being irradiated for 0, 20, and 40 minutes, and the morphology of the bacteria in the three stages was observed with a laser scanning confocal microscope.

3. Results and discussion

3.1 Characterization of materials

The XRD patterns of CuI, CuI–BiOI, BiOI/rGO hydrogel and CuI–BiOI/rGO hydrogel are shown in Fig. 1. It can be seen that all of the characteristic diffraction peaks of CuI appears at 25.5° that is well corresponding to CuI (JCPDS: 06-0246). The characteristic diffraction peaks of BiOI/rGO hydrogel are observed at 24.3°, 29.7°, 31.7° and 49.9°, corresponding to BiOI (JCPDS: 10-0445).[31,32] As for CuI–BiOI/rGO hydrogel, the diffraction peak intensities of BiOI are much stronger than that of CuI, which implied the good crystalline state of BiOI during the thermal treatment process and smaller crystal size of CuI. This suggestion can be confirmed by the morphology and structure of CuI–

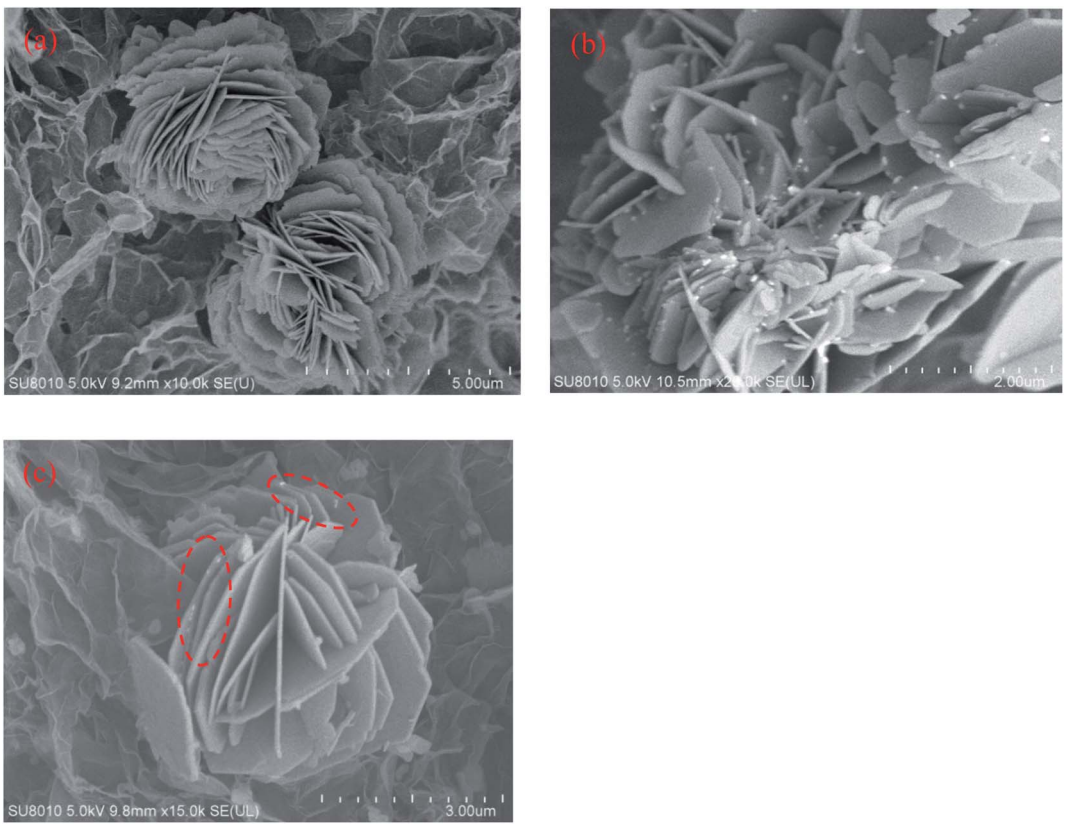

Fig. 2 SEM images of (a) BiOI/rGO hydrogel, and (b) CuI–BiOI powder, (c) CuI–BiOI/rGO hydrogel.

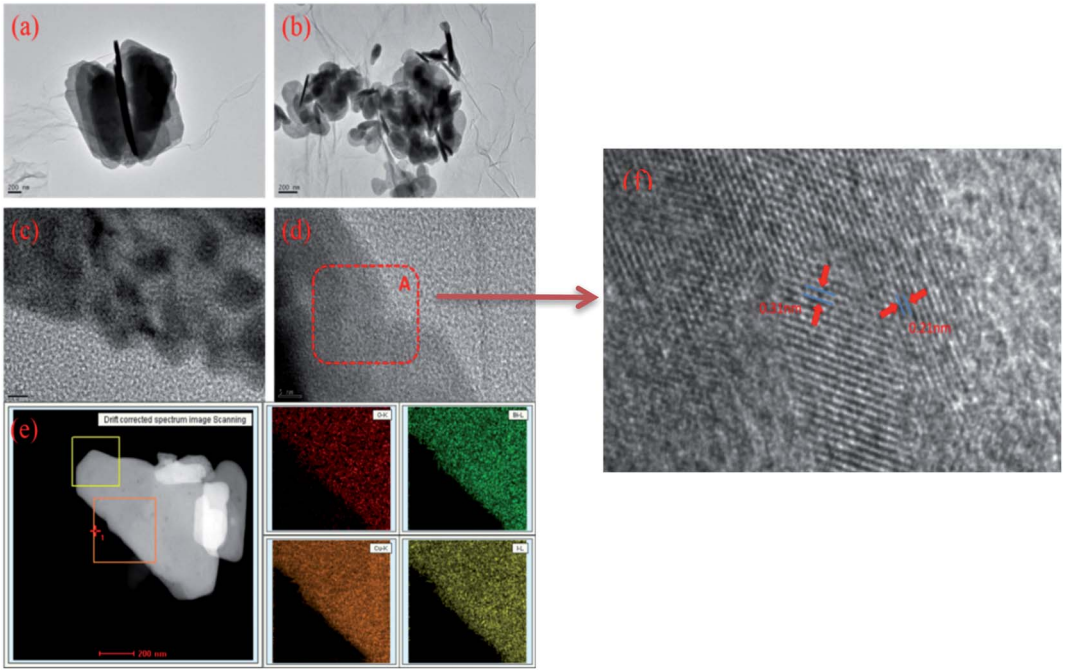

Fig. 3 The TEM (a and b), HRTEM (c and d) and mapping (e) images of CuI–BiOI/rGO hydrogel, (f) the enlarged image of area A in (d).

BiOI/rGO hydrogel test by SEM and TEM, as shown in Fig. 2 and 3. After combine with CuI, the CuI spherical particles uniformly distributed on the surface of BiOI/rGO nanosheets with the intrinsic wrinkle, in comparison to the flower-like nanosheets of bare BiOI/rGO hydrogel sample and CuI–BiOI powder.

The morphology of CuI–BiOI/rGO hydrogel observed by HRTEM are shown in Fig. 3a and b. It can be surveyed that the BiOI sheets cover over the surface of the graphene, and form a close and good interface contact with the graphene. The arrangement of lattice fringes (in Fig. 3c and d) indicates that the composite has a good crystalline state. The lattice spacing at 0.31 nm and 0.21 nm are correspond to the (012) plane of BiOI and the (220) plane of CuI, respectively. In addition, the elements analysis of the CuI–BiOI/rGO hydrogel (in Fig. 3e) shows that the O, Bi, Cu and I elements are evenly dispersed in the sample.

The composition of sample elements, the valence and surface states of individual elements are investigated by XPS.[33] The survey XPS spectrum for CuI–BiOI/rGO hydrogel in Fig. 4a indicates the presence of Bi, O, I, C and Cu elements. For C 1s XPS spectra, the C 1s fitted curves could be assigned to C=C and C–C bonds of the graphene skeleton, C–O (286.1 eV) and C=O (288.5 eV) bonds, respectively.[34,35] The XPS spectrum of Cu 2p shown in Fig. 4c for the composite could be fitted into two absorption peaks centered at 952.3 and 932.4 eV, respectively. But the two signal peaks can't be confirmed to attribute to elemental Cu^{2+} or Cu^{+} ions. Therefore, the attribution of the two signal peaks is distinguished by the Auger spectrum of the Cu element. Normally, when the binding energy is about 570 eV, the corresponding valence of Cu is +1 in the Auger spectrum. For the spectra of Cu LMM, it can be observed that the Cu element has an Auger peak at a binding energy of 570.2 eV, signifying that the Cu element in the CuI–BiOI/rGO hydrogel exists in the +1 valence state. In Fig. 4e, the Bi 4f spectrum shows two obvious peaks locating at 164.2 and 158.9 eV, which are associated with the Bi $4f_{5/2}$ and Bi $4f_{7/2}$ level, respectively. Furthermore, for the XPS of I 3d regions (Fig. 4f), the two typical peaks at binding energies of 630.5 and 619.0 eV can be assigned to the I $3d_{3/2}$ and I $3d_{5/2}$ of I^{-} in CuI–BiOI/rGO hydrogel. As shown in Fig. 4g, the peaks for O 1s at 531.8 eV and 533.8 eV could be assigned to BiOI and rGO.

3.2 Antibacterial properties for *Escherichia coli*

To evaluate the antibacterial activity of different samples, *Escherichia coli* (representative of Gram-negative bacteria) was selected as the template strain for testing. It can be found that all samples showed no significant antibacterial ability under dark conditions from Fig. 5a. Fig. 5b shows that CuI–BiOI powder samples and BiOI/rGO hydrogels exhibited weak antibacterial activity in visible light, while CuI–BiOI/rGO hydrogel showed significant enhanced photocatalytic bacterial activity, which inactivated all bacteria in 40 minutes. In comparison with CuI–BiOI/Cu film which can completely inactivate *E. coli* in 2 h,[16] it has superior antibacterial activity.

The morphological changes of the bacteria during the reaction were further observed by fluorescence staining. The morphology of the bacteria under different reaction times was observed under a laser fluorescence confocal microscope (in Fig. 5c–e). The specific experimental procedures were as follows: bacteria were stained with 4′,6-diamidino-2-phenylindole (DAPI) and pyridine iodide (PI) fluorescent dyes, respectively. DAPI is a fluorescent stain that can stain living cells and emit blue-violet fluorescence under the excitation of laser at the

appropriate wavelength.[36,37] It is a fluorescent stain that can stain living cells. PI is a nuclear staining reagent that can stain DNA and is often used for apoptosis detection. After apoptosis, PI will embed double-stranded DNA to form pi-dna complex and emit red fluorescence.[38–40] In the experiment, the bacterial liquids at different reaction times were collected (0, 20, 40

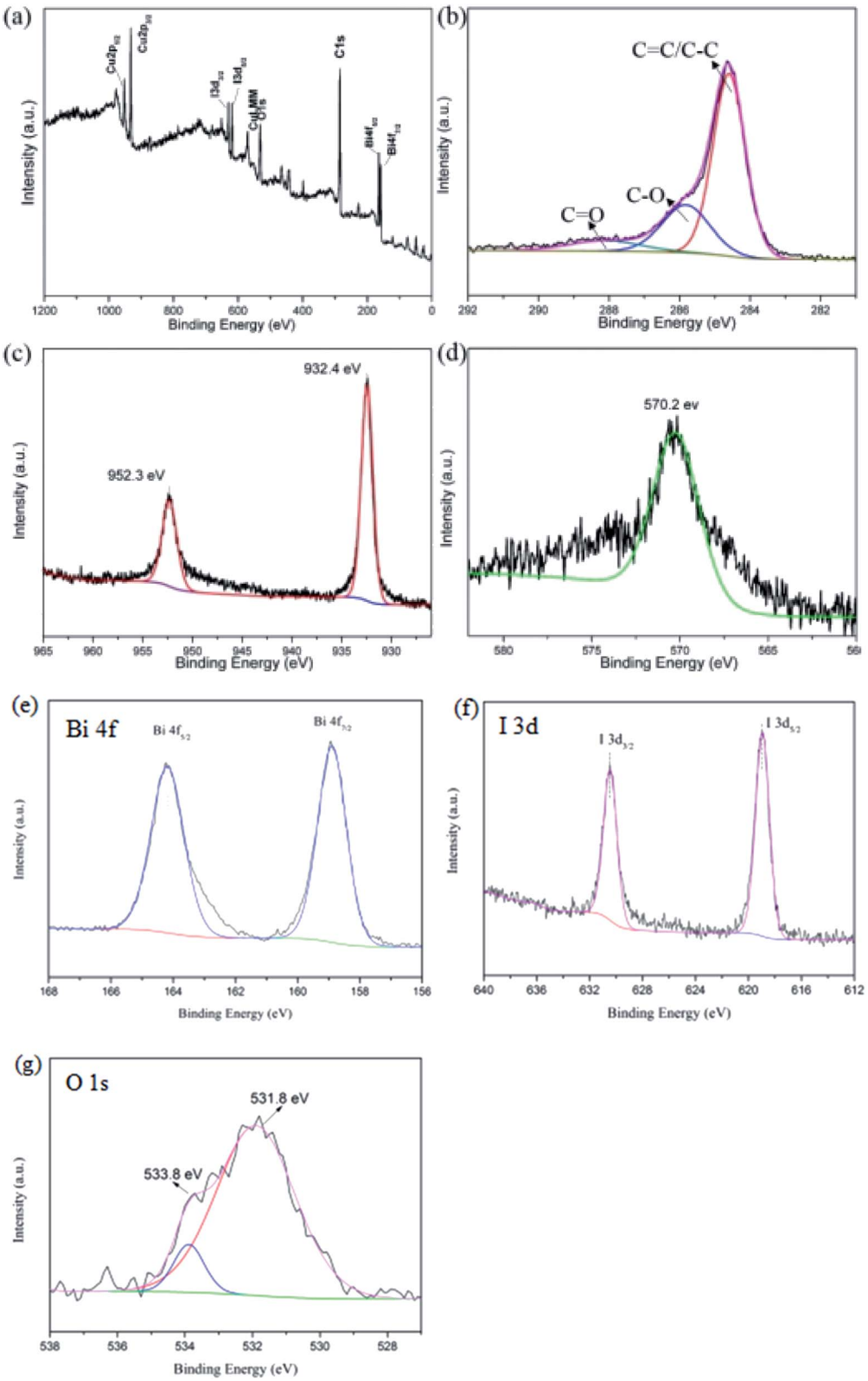

Fig. 4 Overall XPS spectra (a) of samples, high-resolution XPS spectra: (b) C 1s (c) Cu 2p of and (d) Cu LMM (e) Bi 4f (f) I 3d (g) O 1s of CuI–BiOI/rGO hydrogel.

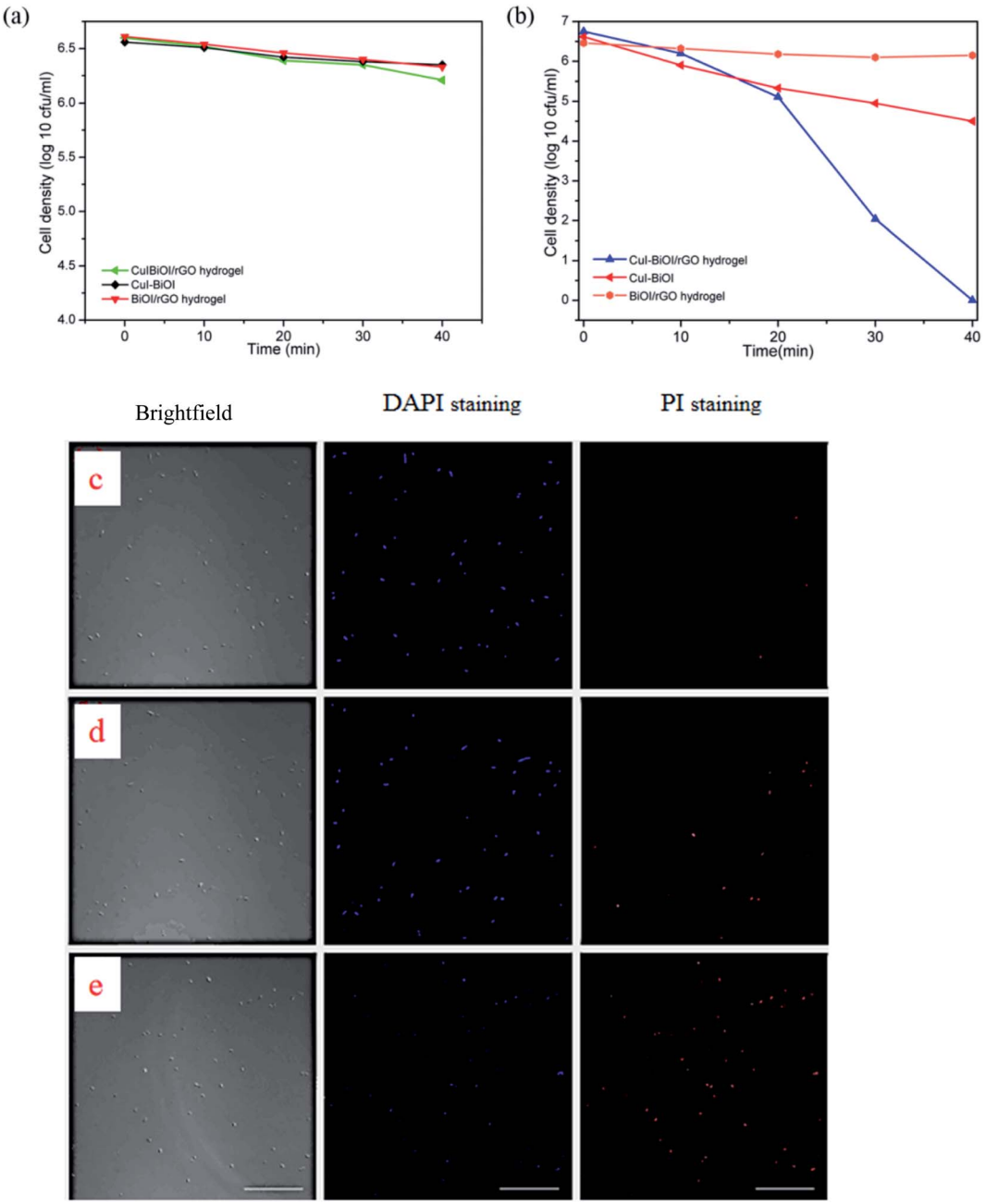

Fig. 5 *E. coli* K – 12 ($10^{6.5}$ CFU mL^{-1}) inactivation by prepared photocatalysts; (a) in the dark and (b) under visible light irradiation ($\lambda \geq 420$ nm); confocal fluorescent images of live and dead *E. coli* under different reaction time (c) 0 min, (d) 20 min, (e) 40 min.

minutes), DAPI solution with a concentration of 5 μg mL^{-1} and PI solution with a concentration of 1 μg mL^{-1} were mixed evenly with the bacterial solution, respectively. After kept for 10 minutes, the excess fluorescence stain was washed away by PBS for several times. Finally, the treated bacteria were observed under a laser fluorescence confocal microscope.

Fig. 5c–e shows the confocal fluorescent images of live and dead *E. coli* under different reaction time (c) 0 min, (d) 20 min, (e) 40 min, respectively. When the reaction time is 0 min, the red fluorescence can hardly be observed, and the bacteria nearly survive normally at this time. The red fluorescence gradually increased as the reaction time was 20 min, indicating that some *E. coli* had died as the reaction progressed. When the reaction time was 40 min, it was observed that the fluorescence produced by DAPI staining and PI staining was almost completely coincident, indicating that *E. coli* had been completely inactivated.

Simultaneously, CuI–BiOI/rGO hydrogel not only exhibits more efficient photocatalytic antibacterial properties, but also allows the macroscopic block structure to be more conveniently recycled for the next reaction after the reaction. Thence, in order to further verify the stability of the CuI–BiOI/rGO hydrogel, the cyclic photocatalytic antibacterial experiment test was carried out. The CuI–BiOI/rGO hydrogel after each reaction was

dialyzed in deionized water for a period of time and then freeze-dried. After collection, the photocatalytic antibacterial performance test was continued. As shown in Fig. S2a,† the results showed that the sample can still inactivate all *E. coli* efficiently within 40 min after five consecutive reactions, indicating that the CuI–BiOI/rGO hydrogel has superior stability and does not decrease its activity as the number of reactions increases. After the reaction, the sample was tested by XRD. Fig. S2b† shows that the XRD patterns of the hydrogel before and after the reaction are basically the same, which proves that the crystal structure of the sample is not destroyed after several cycles of experiments, further indicating that the sample has good stability.

3.3 Antibacterial properties for *Staphylococcus aureus*

According to Gram staining, bacteria can usually be divided into two major categories: Gram-positive bacteria and Gram-negative bacteria. As a representative of Gram-negative bacteria, *Escherichia coli* has been extensively studied as a template bacteria. In order to investigate that the photocatalytic antibacterial property of CuI–BiOI/rGO hydrogel, the representative strain of Gram-positive bacteria: *Staphylococcus aureus* was selected as the model bacterium. In the template bacteria, the antibacterial properties of the prepared CuI–BiOI/rGO hydrogel under visible light were investigated. In Fig. 6, it can be observed that *S. aureus* with an initial concentration of about 10^5 CFU mL^{-1} is almost completely inactivated by CuI–BiOI/rGO hydrogel within 40 min under visible light irradiation. However, both the CuI–BiOI powder sample and the BiOI/rGO hydrogel revealed no obvious sterilization performance under visible light irradiation, and the bacterial concentrations at this time were $10^{4.2}$ and $10^{3.1}$ CFU mL^{-1}, respectively. The results indicate that CuI–BiOI/rGO hydrogel not only has high antibacterial ability against *Escherichia coli*, but also has extremely efficient sterilization performance for *Staphylococcus aureus*.

3.4 Possible photocatalytic antibacterial mechanism

Active free radicals, electrons, holes and H_2O_2, *etc.* can attack bacteria to varying degrees during the photocatalytic antibacterial process. To evaluate the effect of different active species on the photocatalytic activity, different sacrificial agents were added to the CuI–BiOI/rGO hydrogel photocatalytic antibacterial reaction system. Four kinds of sacrificial agents were selected, of which TEMPOL was used as a sacrificial agent for $^{\bullet}O_2^-$, isopropanol was used as a sacrificial agent for $^{\bullet}OH$, Fe(II)–EDTA solution was used as scavenger for H_2O_2, and sodium oxalate was used as scavenger for h^+, Cr(VI) solution as scavenger of e^-. It can be seen from Fig. S3† that the activity of the photocatalytic antibacterial activity of the sample was affected to some extent after the addition of the sacrificial agent and the corresponding active species were removed. The results presented that after adding isopropanol, Fe(II)–EDTA solution and TEMPOL, the sample still showed certain photocatalytic antibacterial activity after exposed to visible light for 40 min (the concentrations of the bacterial liquid were $10^{1.1}$, $10^{2.5}$, $10^{0.7}$, respectively). However, when sodium oxalate and Cr(VI) solution were added to the reaction system, the photocatalytic antibacterial ability of the sample was obviously inhibited and the concentration of the bacterial solution was still $10^{3.7}$ and $10^{4.6}$, revealing that h^+ and e^- were the most important active species in the photocatalytic and antibacterial system of CuI–BiOI/rGO hydrogel. There may be two reasons for this result. On the one hand, h^+ and e^- can directly attack bacteria, resulting in the destruction of bacterial structure and death. On the other hand, the active species such as H_2O_2, $^{\bullet}OH$ and $^{\bullet}O_2^-$ are also produced by h^+ and e^-; $^{\bullet}O_2^-$ is obtained by reducing O_2 by e^-; $^{\bullet}OH$ and H_2O_2 are obtained by oxidizing OH^- in water by h^+. Therefore, as h^+ and e^- are removed, the active species obtained by their redox also disappear accordingly. In general, the separation of photogenerated electrons and holes plays a key role in the photocatalytic antibacterial performance. Accordingly, effective separation of electron–hole pairs is one of the main reasons for the high activity of photocatalyst.[41–44]

To further explore the role of active oxygen in the photocatalytic process, the CuI–BiOI/rGO hydrogel was tested for ESR under dark and light conditions. It can be seen from Fig. S4† that there is almost no signal under dark conditions, but obvious characteristic peaks of $^{\bullet}OH$ and $^{\bullet}O_2^-$ radicals appear under visible light irradiation, which indicates the presence of $^{\bullet}OH$ and $^{\bullet}O_2^-$ radicals in the photocatalytic reaction. What's more, $^{\bullet}O_2^-$ radicals are obtained by reducing O_2 by e^-; $^{\bullet}OH$ radicals are obtained by oxidizing OH^- in water by h^+. This conclusion is consistent with the capture experiment results of different active species.

Photoelectrochemical testing is usually used to evaluate the separation efficiency of h^+ and e^-. The photocurrent is generated by the carriers generated after the photocatalyst is excited by light. To a certain extent, the magnitude of the photocurrent reflects the carrier density generated after the sample is excited by the light, and can be used to judge the charge separation efficiency. The photoelectrochemical performance of CuI–BiOI/rGO hydrogel, BiOI/rGO hydrogel and CuI–BiOI powder catalysts was investigated to probe the reasons for the improvement of photocatalytic performance of CuI–BiOI/rGO hydrogel. Fig. 7 shows the photocurrent response of the three catalysts under visible light irradiation. BiOI/rGO hydrogel has a certain

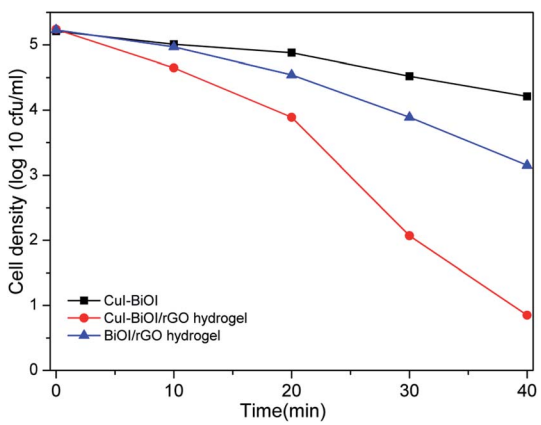

Fig. 6 The photocatalytic inactivation of *S. aureus* by prepared samples under visible light illumination.

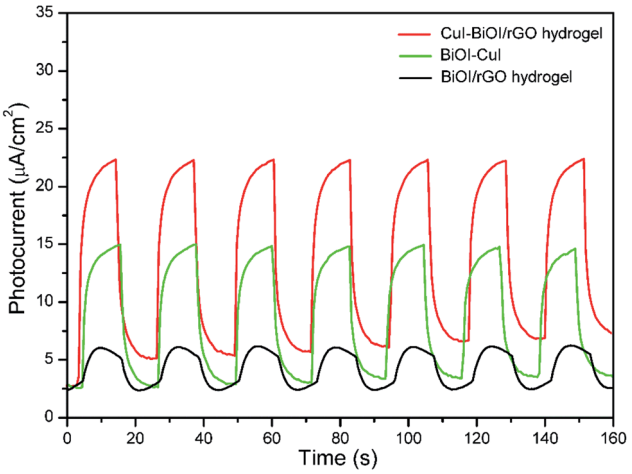

Fig. 7 Transient photocurrent responses of CuI–BiOI/rGO hydrogel, BiOI/rGO hydrogel and CuI–BiOI powders.

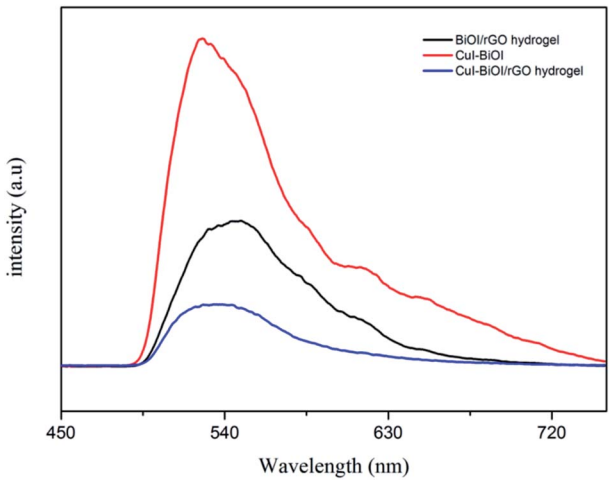

Fig. 8 Photoluminescence spectra with of CuI–BiOI/rGO hydrogel, BiOI/rGO hydrogel and CuI–BiOI powders.

photocurrent response under illumination, yet its photocurrent density is much lower than that of CuI–BiOI/rGO hydrogel under visible light. This is due to the addition of CuI, which significantly increases electrons and holes separation efficiency. Compared with CuI–BiOI catalyst and CuI–BiOI/Cu film,[16] the photocurrent density of CuI–BiOI/rGO hydrogel has been further enhanced. This effect further manifests that GO has a stronger conductive transport capacity than Cu. In terms of photocurrent response, the response value of CuI–BiOI/rGO hydrogel is much higher than that of CuI–BiOI powder catalyst and BiOI/rGO hydrogel, which was in line with antibacterial activity in Fig. 5b and 6.

In addition to photoelectrochemical methods, fluorescence spectra can also reflect the separation of photogenerated carriers.[35] It is generally believed that the stronger the intensity of the fluorescence peak of the sample in the photocatalytic reaction, the more the number of electron holes that are recombined in the photocatalyst, indicating that the carrier separation efficiency in the sample is lower, and accordingly the sample exhibited the poor photocatalytic activity. Fig. 8 shows the fluorescence spectra of CuI–BiOI/rGO hydrogel, BiOI/rGO hydrogel and CuI–BiOI powder catalyst. The results displayed that compared with BiOI/rGO hydrogel and CuI–BiOI powder catalyst, CuI–BiOI/rGO hydrogel renders the lowest fluorescence intensity. It further confirmed that the CuI–BiOI/rGO hydrogel has the highest photocatalytic bacterial inactivation due to the high separation efficiency of electrons and holes in CuI–BiOI/rGO hydrogel samples after photoexcitation with the highest carrier separation efficiency. It coincides with the results in Fig. 5b and 6.

To further investigate the electrons and holes transfer pathway in CuI–BiOI/rGO hydrogel, the band gap of CuI and BiOI is calculated according to the equation:

$$\alpha h\nu = A(h\nu - E_g)^{1/2}$$

where α, $h\nu$, E_g and A are the optical absorption coefficient, photonic energy, band gap and proportionality constant, respectively. From the plot of $(\alpha h\nu)^{1/2}$ *versus* $(h\nu)$ in Fig. S5a,† the E_g of CuI and BiOI were estimated to be 2.86 and 1.84 eV, respectively. It can be seen from Fig. S5b† that the conduction band of CuI is −0.6 eV, and the valence band of CuI and BiOI can be estimated by the following two relations:

$$E_{VB} = \chi - E_e + 0.5E_g$$

$$E_{CB} = E_{VB} - E_g$$

where the χ value of BiOI is 5.99, and E_e (~4.5 eV) is the energy of free electrons on the hydrogen scale. The conduction band and valence band of BiOI can be calculated to be 0.57 eV and 2.41 eV respectively, the valence band of CuI can be calculated to be 2.26 eV.

Based on the above results and discussion, the introduction of CuI and graphene can significantly improve the photocatalytic performance of CuI–BiOI/rGO hydrogel by promoting the separation of photogenerated carriers. As shown in Fig. S6,† due to the good absorption of the complex in the visible region, when exposed to visible light, electrons will be generated in the conduction band (CB) of BiOI, while holes will be generated in the valence band (VB) of BiOI.[26,45,46] At the same time, light-induced electrons promote the reduction of graphene oxide and induce more carbon-centered free radicals, thereby enhancing the antibacterial activity of graphene oxide.[8,9,47] What's more, these electrons can react with a small amount of dissolved oxygen in the solution to form $^{\bullet}O_2^-$. Meanwhile the h^+ from the valence band of BiOI easily transferred to the valence band of CuI, realizing high-efficiency photo-generated carrier separation.[26] Ultimately, The h^+ react with the OH^-/H_2O adsorbed on the surface of the sample to form hydroxyl radicals ($^{\bullet}OH$). These $^{\bullet}OH$ radicals and H_2O_2 with strong oxidation ability will damage the protein and DNA of bacteria, thus changing the physiological structure and metabolic process of bacteria, causing bacterial death.[48,49] Consequently, the photogenic electron hole pairs generated by BiOI can be separated and transferred more effectively *via* the synergistic action of

graphene and CuI, thereby greatly facilitating the photocatalytic antibacterial reaction and further achieving high-efficiency photocatalytic antibacterial activity.

4. Conclusions

In conclusion, CuI–BiOI/rGO hydrogel with high photocatalytic antibacterial activity were prepared by one-step hydrothermal method. It can inactivate all *Escherichia coli* and *Staphylococcus aureus* within 40 min completely. In addition, the CuI–BiOI/rGO hydrogel exhibits good stability which can remain its photocatalytic activity after five cycling experiment. The photoelectron chemistry and fluorescence spectroscopy confirmed that CuI–BiOI/rGO hydrogel has higher separation efficiency for the h^+ and e^- than CuI–BiOI and BiOI/rGO hydrogel. The combination of CuI and rGO hydrogel provides multi-path transfer path for carriers, which greatly increasing the separation efficiency of photogenerated carriers and further achieving more efficient inactivation. This work demonstrated that CuI–BiOI/rGO hydrogel has broad prospects in the practical application of water sterilization.

Conflicts of interest

There are no conflicts to declare.

Acknowledgements

This work was financially supported by the NSFC (Grant no. 21773031), the Science and Technology project of Fujian Province of P. R. China (2020Y4009, 2018H6008), the Natural Science Foundation of Fujian Province of P. R. China (2021H0002).

References

1 K. S. Novoselov, A. K. Geim, S. V. Morozov, D. Jiang, Y. Zhang, S. V. Dubonos, I. V. Grigorieva and A. A. Firsov, Electric field effect in atomically thin carbon films, *Science*, 2004, **306**, 666–669.

2 X. Yang, H. Cui, Y. Li, J. Qin, R. Zhang and H. Tang, Fabrication of Ag_3PO_4-Graphene Composites with Highly Efficient and Stable Visible Light Photocatalytic Performance, *J. Phys. Chem. C*, 2013, **3**, 363–369.

3 S. D. Perera, R. G. Mariano, K. Vu, N. Nour, O. Seitz, Y. Chabal and K. J. Balkus Jr, Hydrothermal Synthesis of Graphene-TiO_2 Nanotube Composites with Enhanced Photocatalytic Activity, *ACS Catal.*, 2012, **2**, 949–956.

4 J. Wang, R. Liu and X. Yin, Adsorptive Removal of Tetracycline on Graphene Oxide Loaded with Titanium Dioxide Composites and Photocatalytic Regeneration of the Adsorbents, *J. Chem. Eng. Data*, 2018, **63**, 409–416.

5 S. Wang, J. Li, S. Wang, J. Wu, T. Wong, M. Foo, W. Chen, K. Wu and G. Xu, Two-Dimensional C/TiO_2 Heterogeneous Hybrid for Noble-Metal-Free Hydrogen Evolution, *ACS Catal.*, 2017, **7**, 6892–6900.

6 W. L. Wang, S. Meng and E. Kaxiras, Graphene nanoFlakes with large spin, *Nano Lett.*, 2008, **8**, 241–245.

7 P. J. Mafa, B. Ntsendwana, B. B. Mamba and A. T. Kuvarega, Visible Light Driven $ZnMoO_4$/$BiFeWO_6$/RGO Z-Scheme Photocatalyst for the Degradation of Anthraquinonic Dye, *J. Phys. Chem. C*, 2019, **123**, 20605–20616.

8 L. Sun, T. Du, C. Hu, J. Chen, J. Lu, Z. Lu and H. Han, Antibacterial Activity of Graphene Oxide/g-C_3N_4 Composite through Photocatalytic Disinfection under Visible Light, *ACS Sustainable Chem. Eng.*, 2017, **5**, 8693–8701.

9 S. Liu, T. Helen Zeng, M. Hofmann, E. Burcombe, J. Wei, R. Jiang, J. Kong and Y. Chen, Antibacterial Activity of Graphite, Graphite Oxide, Graphene Oxide, and Reduced Graphene Oxide: Membrane and Oxidative Stress, *ACS Nano*, 2011, **5**, 6971–6980.

10 Y. Xu, K. Sheng, C. Li and G. Shi, Self-assembled graphene hydrogel *via* a one-step hydrothermal process, *ACS Nano*, 2010, **4**, 4324–4330.

11 N. Katarina, J. Ana, G. Aleksandra Peric, S. Maja Vukašinovic, R. Tamara, Ž. Ljiljana, P. Soo-Jin, R. Kyong Yop and S. J. Vesna Miškovic, Kinetic models of swelling and thermal stability of silver/poly(vinyl/alcohol)/chitosan/graphene hydrogels, *Ind. Eng. Chem.*, 2019, **77**, 83–96.

12 S. Li, J. Zhao, G. Liu, L. Xu, Y. Tian, A. Jiao and M. Chen, Graphene oxide-grafted plasmonic Au@Ag nanoalloys with improved synergistic effects for promoting hot carrier-driven photocatalysis under visible light irradiation, *Nanotec*, 2021, **32**, 125401.

13 Z. Lu, L. Wu, J. Zhang, W. Dai, G. Mo and J. Ye, Bifunctional and highly sensitive electrochemical non-enzymatic glucose and hydrogen peroxide biosensor based on $NiCo_2O_4$ nanoflowers decorated 3D nitrogen doped holey graphene hydrogel, *Mater. Sci. Eng., C*, 2019, **102**, 708–717.

14 L. Shen, Z. Jin, W. Xu, X. Jiang, Y. Shen, Y. Wang. and Y. Lu, Enhanced Treatment of Anionic and Cationic Dyes in Wastewater through Live Bacteria Encapsulation Using Graphene Hydrogel, *Ind. Eng. Chem. Res.*, 2019, **58**, 7817–7824.

15 Y. Liao, M. Wang and D. Chen, Electrosorption of uranium(VI) by highly porous phosphate-functionalized graphene hydrogel, *Appl. Surf. Sci.*, 2019, **484**, 83–96.

16 Y. Zhang, C. Lin, Q. Lin, Y. Jin, Y. Wang, Z. Zhang, H. Lin, J. Long and X. Wang, CuI-BiOI/Cu film for enhanced photo-induced charge separation and visible-light antibacterial activity, *Appl. Catal., B*, 2018, **235**, 238–245.

17 J. Liang, J. Deng, M. Li, T. Xu and M. Tong, Bactericidal activity and mechanism of Ti-doped BiOI microspheres under visible light irradiation, *Colloids Surf., B*, 2016, **147**, 307–314.

18 X. Wang, C. Zhou, L. Yin, R. Zhang and G. Liu, Iodine-Deficient BiOI Nanosheets with Lowered Valence Band Maximum To Enable Visible Light Photocatalytic Activity, *ACS Sustainable Chem. Eng.*, 2019, **7**, 7900–7907.

19 M. Padervand, E. Jalilian, R. Majdani and M. Goshadezehn, BiOCl/AgCl-BiOI/AgI quaternary nanocomposite for the efficient photodegradation of organic wastewaters and

pathogenic bacteria under visible light, *J. Water Process Eng.*, 2019, **29**, 100789.

20 L. Ye, X. Liu, Q. Zhao, H. Xie and L. Zan, Dramatic visible light photocatalytic activity of MnOx-BiOI heterogeneous photocatalysts and the selectivity of the cocatalyst, *J. Mater. Chem. A*, 2013, **1**, 8978–8983.

21 Q. Liang, S. Cui, J. Jin, C. Liu, S. Xu, C. Yao and Z. Li, Fabrication of BiOI@UIO-66(NH_2)@g-C_3N_4 ternary Z-scheme heterojunction with enhanced visible-light photocatalytic activity, *Appl. Surf. Sci.*, 2018, **456**, 899–907.

22 J. Liang, C. Shan, X. Zhang and M. Tong, Bactericidal mechanism of BiOI-AgI under visible light irradiation, *Chem. Eng. J.*, 2015, **279**, 277–285.

23 J. Wu, X. Chen, C. Li, Y. Qi, X. Qi, J. Ren, B. Yuan, B. Ni, R. Zhou, J. Zhang and T. Huang, Hydrothermal synthesis of carbon spheres – BiOI/$BiOIO_3$ heterojunctions for photocatalytic removal of gaseous Hg^0 under visible light, *Chem. Eng. J.*, 2016, **304**, 533–543.

24 D. Kandi, S. Martha, A. Thirumurugan and K. M. Parida, Modification of BiOI Microplates with CdS QDs for Enhancing Stability, Optical Property, Electronic Behavior toward Rhodamine B Decolorization, and Photocatalytic Hydrogen Evolution, *J. Phys. Chem. C*, 2017, **121**, 4834–4849.

25 L. Sun, L. Xiang, X. Zhao, C. Jia, J. Yang, Z. Jin, X. Cheng and W. Fan, Enhanced Visible-Light Photocatalytic Activity of BiOI/BiOCl Heterojunctions: Key Role of Crystal Facet Combination, *ACS Catal.*, 2015, **5**, 3540–3551.

26 M. Sun, J. Hu, C. Zhai, M. Zhu and J. Pan, CuI as Hole-Transport Channel for Enhancing Photoelectrocatalytic Activity by Constructing CuI/BiOI Heterojunction, *ACS Appl. Mater. Interfaces*, 2017, **9**, 13223–13230.

27 S. Yoon, H. Kim, E. Y. Shin, I. G. Bae, B. Park, Y. Y. Noh and I. Hwang, Enhanced Hole Extraction by Interaction between CuI and MoO_3 in the Hole Transport Layer of Organic Photovoltaic Devices, *Org. Electron.*, 2016, **32**, 200–207.

28 K. Tennakone, V. P. S. Perera, I. R. M. Kottegoda and G. R. R. A. Kumara, Dye-Sensitized Solid State Photovoltaic Cell Based on Composite Zinc Oxide/Tin (IV) Oxide Films, *J. Phys. D: Appl. Phys.*, 1999, **32**, 374–379.

29 M. Rusop, T. Shirata, P. M. Sirimanne, T. Soga, T. Jimbo and M. Umeno, Study on the Properties and Charge Generation in DyeSensitized n-TiO_2|Dye|p-CuI Solid State Photovoltaic Solar Cells, *Appl. Surf. Sci.*, 2006, **252**, 7389–7396.

30 K. Tennakone, G. R. R. A. Kumara, I. R. M. Kottegoda, K. G. U. Wijayantha and V. P. S. Perera, A Solid-State Photovoltaic Cell Sensitized with a Ruthenium Bipyridyl Complex, *J. Phys. D: Appl. Phys.*, 1998, **31**, 1492–1496.

31 Y. Yang, H. Yin, H. Li, Q. Zou, Z. Zhang, W. Pei, L. Luo, Y. Huo and H. Li, Synergistic Photocatalytic-Photothermal Contribution to Antibacterial Activity in BiOI-Graphene Oxide Nanocomposites, *ACS Appl. Bio Mater.*, 2018, **1**, 2141–2152.

32 F. Rao, G. Zhu, M. Hojamberdiev, W. Zhang, S. Li, J. Gao, F. Zhang, Y. Huang and Y. Huang, Uniform Zn^{2+}-Doped BiOI Microspheres Assembled by Ultrathin Nanosheets with Tunable Oxygen Vacancies for Super-Stable Removal of NO, *J. Phys. Chem. C*, 2019, **123**, 16268–16280.

33 J. Jiang, X. Zhang, P. Sun and L. Zhang, ZnO/BiOI Heterostructures: Photoinduced Charge-Transfer Property and Enhanced Visible-Light Photocatalytic Activity, *J. Phys. Chem. C*, 2011, **115**, 20555–20564.

34 R. Wang, K. Lu, F. Zhang, Z. Tang and Y. Xu, 3D carbon quantum dots/graphene aerogel as a metal-free catalyst for enhanced photosensitization efficiency, *Appl. Catal., B*, 2018, **233**, 11–18.

35 B. Liu, X. Han, Y. Wang, X. Fan, Z. Wang, J. Zhang and H. Shi, Synthesis of g-C_3N_4/BiOI/BiOBr heterostructures for efficient visible-light-induced photocatalytic and antibacterial activity, *J. Mater. Sci.: Mater. Electron.*, 2018, **29**, 14300–14310.

36 A. A. Oleksienko, Y. G. Kot and V. P. Komaristaya, DNA-Specific DAPI Staining of the Pyrenoid Matrix During its Fission in Dunaliella salina (Dunal) Teodoresco (Chlorophyta), *Curr. Microbiol.*, 2020, **77**, 3450–3459.

37 M. Terashima, Y. Kamagata and S. Kato, Rapid Enrichment and Isolation of Polyphosphate-Accumulating Organisms Through 4'6-Diamidino-2-Phenylindole (DAPI) Staining With Fluorescence-Activated Cell Sorting (FACS), *Front. Microb.*, 2020, **11**, 793.

38 S. Kasibhatla, G. P Amarante-Mendes, D. Finucane, T. Brunner, E. Bossy-Wetzel and D. R Green, Analysis of DNA Fragmentation Using Propidium Iodide (PI) Staining After Ethanol Fixation, *CSH Protoc.*, 2006, **1**, 4431.

39 L. Rodgers, Measurement of DNA Content Using Propidium Iodide (PI) Staining of Fixed Whole Cells, *CSH Protoc.*, 2006, **1**, 4436.

40 G. Vartholomatos, G. A. Alexiou, K. Stefanakic, E. G. Lykoudis, G. Tseka, M. Tzoufi, G. Sfakianos and N. Prodromou, The value of cell cycle analysis by propidium-iodine staining of CD56+ cells in pediatric brain tumors, *Clinical Neurology and Neuroscience*, 2015, **133**, 70–74.

41 L. Zhu, C. He, Y. Huang, Z. Chen, D. Xia, M. Su, Y. Xiong, S. Li and D. Shu, Enhanced photocatalytic disinfection of *E. coli* 8099 using Ag/BiOI composite under visible light irradiation, *Sep. Purif. Technol.*, 2012, **91**, 59–66.

42 Y. Yang, H. Yin, H. Li, Q. Zou, Z. Zhang, W. Pei, L. Luo, Y. Huo and H. Li, Synergistic Photocatalytic-Photothermal Contribution to Antibacterial Activity in BiOI-Graphene Oxide Nanocomposites, *ACS Appl. Bio Mater.*, 2018, **1**, 2141–2152.

43 Y. Jin, J. Long, X. Ma, T. Zhou, Z. Zhang, H. Lin, J. Long and X. Wang, Synthesis of caged iodine-modified ZnO nanomaterials and study on their visible light photocatalytic antibacterial properties, *Appl. Catal., B*, 2019, **256**, 117873.

44 W. Deng, S. Ning, Q. Lin, H. Zhang, T. Zhou, H. Lin, J. Long, Q. Lin and X. Wang, I-TiO_2/PVC film with highly photocatalytic antibacterial activity under visible light, *Appl. Catal., B*, 2016, **144**, 196–202.

45 Q. Wang, X. Shi, E. Liu, J. C. Crittenden, X. Ma, Y. Zhang and Y. Cong, Facile Synthesis of AgI/BiOI-Bi_2O_3, MultiHeterojunctions with High Visible Light Activity for Cr(VI) Reduction, *J. Hazard. Mater.*, 2016, **317**, 8–16.

46 M. Arumugam, S. J. Lee, T. Begildayeva, S. S. Naik, Y. Yu, H. Lee, J. Theerthagiri and M. Y. Choi, Enhanced photocatalytic activity at multidimensional interface of 1D-Bi_2S_3@2D-GO/3D-BiOI ternary nanocomposites for tetracycline degradation under visible-light, *J. Hazard. Mater.*, 2021, **404**, 123868.

47 Y. Chong, C. Ge, G. Fang, R. Wu, H. Zhang, Z. Chai, C. Chen and J. Yin, Light-Enhanced Antibacterial Activity of Graphene Oxide, Mainly *via* Accelerated Electron Transfer, *Environ. Sci. Technol.*, 2017, **51**, 10154–10161.

48 M. Zhang, X. Hou, L. Lv, Y. Wang, C. Li and A. Meng, Synthesis of Ag/AgCl modified anhydrous basic bismuth nitrate from BiOCl and the antibacterial activity, *Mater. Sci. Eng., C*, 2019, **98**, 83–88.

49 D. K. Padhi, T. K. Panigrahi, K. Parida, S. K. Singh and P. M. Mishra, Green Synthesis of Fe_3O_4/RGO Nanocomposite with Enhanced Photocatalytic Performance for Cr(VI) Reduction, Phenol Degradation, and Antibacterial Activity, *ACS Sustainable Chem. Eng.*, 2017, **5**, 10551–10562.